Eur. Phys. J. B **37**, 285–292 (2004)
DOI: 10.1140/epjb/e2004-00058-4

THE EUROPEAN PHYSICAL JOURNAL B

$La_{0.5}Sr_{0.5}CoO_3$: A ferromagnet with strong irreversibility

A. Senchuk, H.P. Kunkel, R.M. Roshko[a], C. Viddal, Li Wei, G. Williams, and X.Z. Zhou

Department of Physics and Astronomy, University of Manitoba Winnipeg MB Canada R3T 2N2

Received 19 August 2003
Published online 2 April 2004 –

Abstract. This paper presents a summary of measurements of the field and temperature dependence of the ac susceptibility, magnetic hysteresis isotherms, and the zero field cooled (ZFC) and field cooled (FC) moment. These results demonstrate that $La_{0.5}Sr_{0.5}CoO_3$ is consistently and comprehensively described as a ferromagnet with strong irreversibility. Analysis of the ac susceptibility demonstrates unequivocally the occurrence of a continuous (second order) paramagnetic to ferromagnetic phase transition with mean-field-like *effective* exponents (although estimates for the true, asymptotic critical exponents appear precluded by the substantial anisotropy/coercivity, linked to the presence of Co ions). The behaviour of the irreversible response is analyzed within the framework of a Preisach model which decomposes the magnetizing process into a sequence of two-state Barkhausen excitations. The model is able to replicate the field and temperature dependence of the hysteresis isotherms and the FC and ZFC moments, and shows that these response functions are a product of field activated transitions over a spectrum of temperature dependent metastable state excitation barriers, with a negligible contribution from thermal fluctuations.

PACS. 75.40.-s Critical-point effects, specific heats, short-range order – 75.40.Cx Static properties (order parameter, static susceptibility, heat capacities, critical exponents, etc.) – 75.60.Ej Magnetization curves, hysteresis, Barkhausen and related effects – 75.50.Cc Other ferromagnetic metals and alloys

1 Introduction

The (re)discovery of colossal magnetoresistance (CMR) in the manganese perovskites (general formula $A_{1-x}B_xMnO_3$, where A is typically La, Y or another rare-earth ion and B a divalent cation) has resulted in their becoming – along with their cuprate counterparts exhibiting high temperature superconductivity – some of the most intensively studied compounds over roughly the past decade [1].

While the $La_{1-x}Sr_xCoO_3$ system has not been as extensively studied of late as its Mn perovskite counterpart, nevertheless its magnetic, transport and related properties have been widely reported ([2–5] and references listed therein). Despite such investigations the magnetic properties, in particular, remain the subject of disparate interpretation, as do those of the Mn perovskite family [6]. Some of these differences have been attributed to thermally induced changes in the spin state of Co ions, variously designated as Low Spin (LS, $t_{2g}^6(\sigma^*/e_g)^0$, $S = 0$), Intermediate Spin (IS, $t_{2g}^5e_g^1$, $S = 1$) or High Spin (HS, $t_{2g}^6e_g^2$, $S = 2$) [2–4]. However, for Sr content $x > 0.2$, current consensus appears to support the appearance of bulk ferromagnetism below $T_C \approx 230$ K (see, for example, Ref. [4]), linked possibly with the suggestion that increased Sr doping stabilizes the IS configuration. Nevertheless, the behaviour of specimens with $x > 0.2$ has also been categorized [3] as ferromagnetic + cluster glass (FM + CG), despite the fact that neutron scattering data indicate the occurrence of *long range ferromagnetism* with correlation lengths in excess of hundreds of Å̊s [2,7], a conclusion supported by calorimetric studies [8]. Thus, some uncertainties still prevail in the description of the doping region $0.2 < x \lesssim 0.5$, with several references to so called glassy ferromagnetic behaviour. While the latter originate principally from perceived anomalies in the dynamic magnetic response (a strong frequency dependence in χ' and structure in χ'') [2,9], ancillary effects have been identified in the field dependence of the maximum in the zero-field-cooled magnetisation. In particular, these maxima have been attributed to the presence of considerable magnetocrystalline anisotropy in this system [3,9,10], and a phenomenological expression suggested to account for some of these anisotropy induced effects [10].

Here we present a summary of extensive measurements of the field and temperature dependence of the real part of the ac susceptibility, magnetic hysteresis isotherms, and the zero-field cooled (ZFC) and field-cooled (FC) magnetisation of the prototypical compound $La_{0.5}Sr_{0.5}CoO_3$. These data are analysed quantitatively in terms of specific models, enabling the former measurements to be utilized to demonstrate the occurrence of a continuous (second order) paramagnetic to ferromagnetic phase transition (confirming the earlier conclusions of Menyuk et al. [11]), and

[a] e-mail: roshko@cc.umanitoba.ca

to deduce the associated critical exponents. Confirmation of the true, asymptotic values for the latter are, however, precluded by the substantial anisotropy/coercivity mentioned above, a point discussed in more detail below. The behaviour of the FC and ZFC magnetisation and the irreversible response is analysed within the framework of a model which decomposes the magnetising process into a sequence of two-state Barkhausen excitations. As in related perovskites, oxygen stoichiometry can play an important role in aspects of the behaviour of this system, particularly for compositions $x > 0.3$ [12]. It is not, however, our intention to produce specimens with precisely defined composition, rather to produce a sample(s) with magnetic properties closely replicating those displayed by samples of the same nominal composition produced by other investigators, analysing such properties in the manner outlined above. The results of this approach demonstrate that $La_{0.5}Sr_{0.5}CoO_3$ is consistently and comprehensively described as a ferromagnet with strong irreversibility.

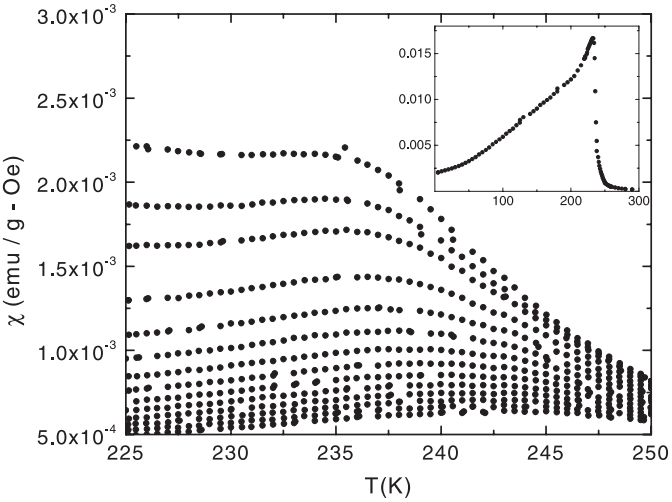

Fig. 1. The ac susceptibility (in emu/g-Oe) corrected for background and demagnetizing effects plotted against temperature T (in K), measured in superimposed static biasing fields increasing from 1 kOe (top) to 7 kOe (bottom). The insert shows the corresponding zero field ac susceptibility.

2 Experimental details

Samples of nominal composition $La_{0.5}Sr_{0.5}CoO_3$ were prepared using standard ceramic techniques. Stoichiometric quantities of La_2O_3 (99.99% purity) $SrCO_3$ and Co_3O_4 were thoroughly mixed and ground for 24 h. by ball milling in acetone. The dried powder was subsequently pressed into pellet form and fired at 900 °C for 24 h. The pellet was then reground, mixed with an inert binder, and then refired in flowing oxygen for 24 hours at 1000 °C followed by 96 h. at 1050 °C, the latter being close to that adopted in several previous studies [2]. Powder X-ray diffraction using Cu-K_{alpha} radiation indicated a single phase compound and could be indexed to a pseudo-cubic perovskite-like cell with lattice constant $a = 3.838(4)$ Å; the latter is in good agreement with previous reports [2,3] confirming a composition close to the nominal value [5]. SEM measurements yield a typical grain size of $\sim$1 μm.

Ac susceptibility and dc magnetization data were acquired as a function of both field and temperature using a Quantum Design PPMS model 6000 magnetometer/susceptometer on a sample of approximate dimensions $(6 \times 1 \times 1)$ mm^3 cut from the final pellet, with magnetic fields always applied parallel to the long axis.

3 Results and discussion

3.1 Behaviour in the vicinity of T_C

The insert in Figure 1 shows the temperature dependence of the zero field ac susceptibility $\chi(0,T)$, measured on warming, following zero field cooling, at 2.4 kHz with a driving field amplitude of 30 mOe applied parallel to the longest dimension. No thermal hysteresis was detected in the measurement. $\chi(0,T)$, corrected for background and demagnetizing effects, increases abruptly with decreasing temperature below 250 K, then exhibits a maximum, the Hopkinson peak [13], *below* the ferromagnetic ordering temperature T_C (as the following analysis confirms) after which it decreases smoothly as the temperature is lowered further. The data in the main body of Figure 1 shows the corresponding temperature dependent susceptibility in static fields H_a applied parallel to the ac driving field, increasing from 1 kOe (top) to 7 kOe (bottom). With increasing H_a, the principal Hopkinson maximum is suppressed in both amplitude and temperature, enabling a set of secondary peaks (at temperatures designated T_m) to be observed near 240 K in the susceptibility $\chi(H_a,T)$. These latter peaks, which decrease in amplitude and move upward in temperature as H_a increases, reflect the presence of critical fluctuations accompanying a continuous transition to a ferromagnetic state and their presence can be understood on the basis of the fluctuation-dissipation theorem [14]. They are a feature predicted by the static scaling law [15], from Monte Carlo simulations on the three-dimensional Heisenberg model [16] and by numerical calculations on mean-field models [17]. A detailed analysis of the field and temperature dependence of these peaks yields estimates for the usual critical exponents γ, β and δ, as discussed previously for metallic, amorphous and semiconducting systems [15,18–20]. Consequently, the principal conclusions alone are summarized below. What needs to be reiterated here however is that conventional critical point analysis (the approach utilised previously to estimate γ and δ for this system at this [11] and other [21] compositions) is usually based on the use of modified Arrott plots at fixed temperatures) from which the spontaneous magnetization and inverse initial susceptibility are found by extrapolation from finite field (often hundreds of Oersteds to one or two kOe) [6,11,21]. Such an approach avoids the asymptotically low field region (and, to a lesser extent, the low reduced temperature region) which is precisely the regime of validity of the static scaling law.

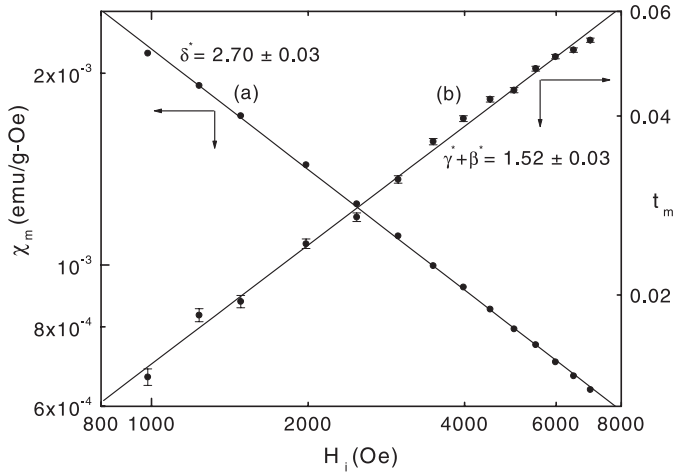

Fig. 2. (a) The critical peak amplitude taken directly from Figure 1 plotted against the internal field H_i on a double-logarithmic scale. The solid line yields the δ^* value shown. (b) A double-logarithmic plot of the (reduced) critical peak temperature taken from Figure 1 against the internal field. The solid line corresponds to the value of $\gamma^* + \beta^*$ shown.

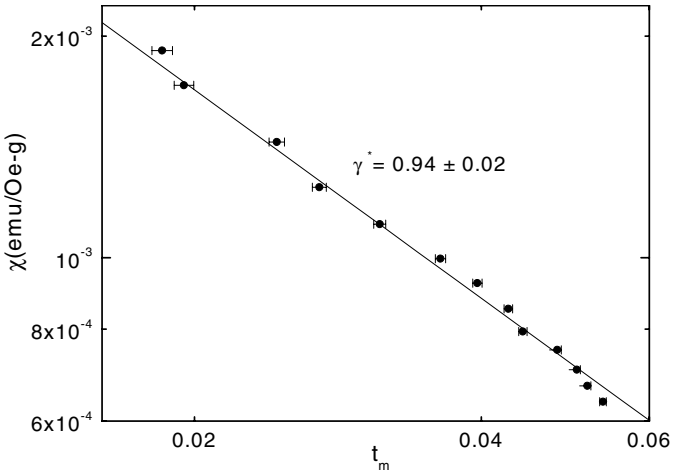

Fig. 3. The critical peak amplitude taken directly from Figure 1 plotted on a double-logarithmic scale against the (reduced) critical peak temperature taken from the same figure. The straight line yields the γ^* value indicated.

This procedure is adopted because the measured response unavoidably contains both critical and non-critical contributions. The former – the singular component arising from critical fluctuations – is what needs to be used in a comparative analysis with scaling law predictions. The latter, also called the regular or technical response, arising from processes such as domain wall motion, coherent rotation, etc., do not form part of such analysis, and hence need to be removed. This can be accomplished by driving the system to "technical saturation", an extrapolation from which eliminates the corresponding component. This is the philosophy behind the modified Arrott plot extrapolation procedure [18], and while it is unquestionably necessary, there is no quantitative criterion that can be applied which ensures that the technical contribution is indeed saturated and the critical component dominates the subsequently measured response. The technique adopted here avoids this difficulty; when the critical peak structure evident in Figure 1 appears, there is no question that the critical response dominates; the limitations to this technique (discussed in more detail below) is that the critical behaviour cannot be assessed in regimes where these peaks are masked by the (unsaturated) technical response.

Figure 2a shows the critical peak amplitude $\chi(H_i, T_m)$ obtained directly from Figure 1 plotted against the internal field $H_i (= H_a - NM$, where N is the demagnetizing factor and M is the magnetization) on a double logarithmic scale. (N was estimated by approximating the sample by an ellipsoid with principal axes equal to the dimensions given above, and then evaluating the corresponding elliptic integral [22]. This procedure is necessary because the field dependence of the magnetization does not "shear".) The scaling law predicts a power law relationship between these two quantities given by [15–20]

$$\chi(H_i, T_m) \propto H_i^{1/\delta - 1} \tag{1}$$

which enables an estimate for δ to be made, *independent of any knowledge of, or a choice for,* T_C, a second advantage of this technique. The straight line drawn in this figure confirms the power law prediction of the above equation, while a least squares fit yields a slope from which the (effective) exponent δ^* (discussed below) is found to be:

$$\delta^*(H) = 2.70 \pm 0.03 \text{ for } 1 \text{ kOe} \leq H_i \leq 8 \text{ kOe}.$$

Close examination of Figure 2a reveals slight curvature, with data points at *higher* field yielding *higher* (effective) exponent values. Fitting to the seven highest field points in this figure yields:

$$\delta^*(H) = 2.93 \pm 0.04 \text{ for } 4 \text{ kOe} \leq H_i \leq 8 \text{ kOe}.$$

Both of these estimates are close to mean-field model predictions.

These same approaches [15–20] relate the temperature T_m of the critical peak maxima obtained directly from Figure 1 to the (internal) field via

$$t_m = \frac{T_m - T_C}{T_C} \propto H_i^{(\gamma+\beta)^{-1}} \tag{2}$$

and to the field dependent peak susceptibility $\chi(H_i, T_m)$ as:

$$\chi(H_i, T_m) \propto t_m^{-\gamma}. \tag{3}$$

Both of these power law relationships can only be tested once a choice for T_C has been made, in contrast to equation (1). This choice is made by initially plotting T_m against $H_i^{(\gamma+\beta)^{-1}}$, with the $H_i = 0$ intercept providing a first estimate for $T_C = 230.9 \pm 0.2$ K [23]. The double logarithmic plots of t_m vs. H_i in Figure 2b, and of the critical peak amplitude $\chi(H_i, T_m)$, obtained directly from Figure 1, against t_m, shown in Figure 3, utilize this estimate. The least squares fitted straight lines drawn in

these figures verify the power law relationships contained in equations (2) and (3), and yield:

$$(\gamma^* + \beta^*) = 1.52 \pm 0.03 \text{ for } 1 \text{ kOe} \leq H_i \leq 8 \text{ kOe}$$
$$\gamma^* = 0.94 \pm 0.02 \text{ for } 1.9 \times 10^{-2} \leq t_m \leq 6 \times 10^{-2}.$$

As with Figure 2a, a fit to the data above $t_m \sim 3 \times 10^{-2}$ in Figure 3 yields:

$$\gamma^* = 1.02 \pm 0.05.$$

All of the above have been designated as effective exponent values due to the reduced temperature (t) and field range accessed by the present experiment, a limitation that is encountered in evaluating critical exponents from measurements following the crossover line in systems where technical saturation is not easily accomplished. (By contrast, in technically soft systems, PdFe [24], for example, such measurements can be extended to very small fields ≈ 0.04 Oe.) Nevertheless the present estimate for T_C is in very good agreement with that estimated by Menyuk et al. [11] ($T_C = 228.4$) using conventional Arrott plot techniques on a sample with the same nominal composition; similarly, both the current and these previous measurements yield estimates for δ ($= 3.05 \pm 0.06$ [11]) close to the mean-field prediction, while the present approach yields an estimate for γ (and β) more consistent with the same model prediction than did the earlier studies ($\gamma = 1.27 \pm 0.022$ [11]). Whether this reflects the use of differing techniques is difficult to resolve, especially as both sets of exponent estimates were extracted from data obtained exclusively above T_C, and hence *cannot* be influenced by any possible spin configuration modification that might occur *at* T_C [21]. Furthermore, the final choice for T_C adopted above places it *above* the principal Hopkinson maximum in the zero-field susceptibility, as is usual [13], in contrast to those reported in reference [21] for samples with lower Sr content. The (effective) exponent values reported above are thus approximately consistent with earlier estimates for γ and δ using complementary techniques on a specimen of the same nominal composition, and with mean-field model predictions (more correctly, the latter model, as well as the Ising model subject to dipole-dipole interactions [25]). While this result disagrees with recent predictions of Heisenberg like behaviour in double-exchange (DE) dominated systems [26], experimental data on a wide range of related materials, including Mn perovskite films [27] and bulk polycrystalline ceramic samples [28] also yield similar exponent values to those reported above (and in the case of films, is accompanied by a more elaborate discussion of theoretically predicted behaviour, which is therefore not repeated here). In the case of bulk LaSrMnO however, single crystal [6,29] critical exponent estimates differ from the quasi mean-field values found in polycrystals, a result that has recently been discussed in terms of the possibility of crossover (3D Ising/Heisenberg to mean-field) induced by a finite polycrystalline grain size [6]. However given the much larger grain size of ~ 1 μm, this seems a very unlikely scenario for the present system (all other parameters being equal).

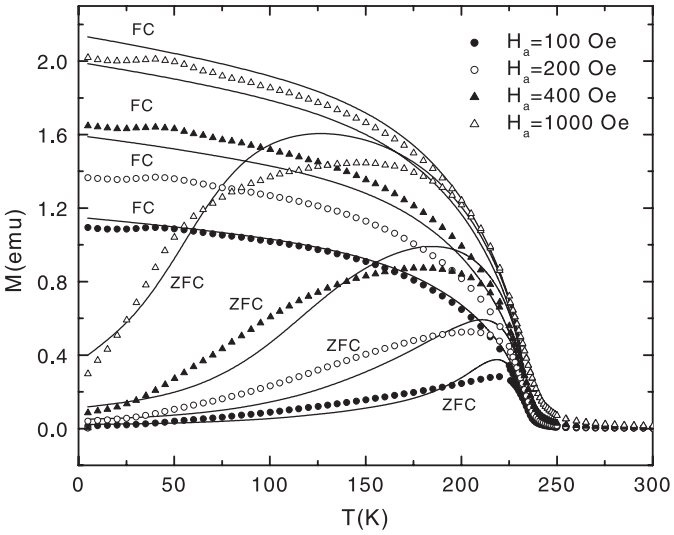

Fig. 4. Measurements (discrete points) and numerical simulations (solid curves) of the FC and ZFC moment as a function of temperature in four applied fields H_a.

Given the importance of the technical components in the magnetization in assessing these critical exponents, a detailed appraisal of their behaviour is presented below.

3.2 Characterizing the irreversible response

The irreversible response of the system was characterized experimentally by measuring (a) the temperature dependence of the total moment $M(T)$, under both field cooled (FC) and zero field cooled (ZFC) conditions, over a temperature interval 5 K $\leq T \leq$ 300 K which encompasses the entire ordered phase, in a wide range of applied fields between 50 Oe $\leq H_a \leq$ 1000 Oe, and (b) major hysteresis loop isotherms in fields between -20 kOe $\leq H_a \leq +20$ kOe, up to technical saturation, over a broad range of temperatures 5 K $\leq T < T_C$ which also spans the ordered phase. Figure 4 shows some representative ZFC and FC data (discrete points), measured on warming from $T = 5$ K in various external fields H_a, after first cooling from $T = 300$ K in zero field and in the external field, respectively. The FC and ZFC branches display a pronounced bifurcation below T_C, which is particularly apparent in low applied fields. The temperature dependence of the ZFC branch is characterized by a maximum, which becomes progressively broader and shifts to lower temperatures in response to increases in H_a. The FC branch has a temperature dependence which is monotonic and which has essentially the same shape in all fields. FC-ZFC thermal bifurcation always coexists with hysteresis in magnetizing isotherms, and Figure 5 shows some representative measured major loop isotherms (discrete points), at several different temperatures, selected so as to illustrate the systematic collapse of the saturation moment, the saturation remanence, and the coercive field as the system is warmed through the ordered phase towards T_C. The solid

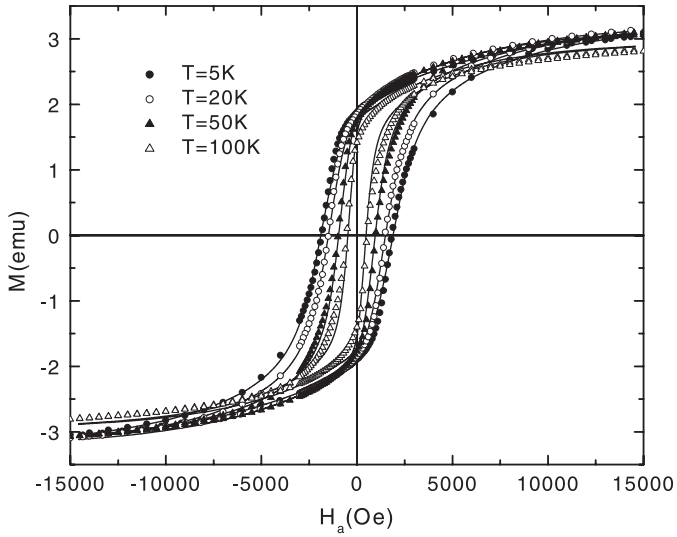

Fig. 5. Measurements (discrete points) and numerical simulations (solid curves) of major hysteresis isotherms at four representative temperatures T.

curves in Figures 4 and 5 represent model simulations described below.

Irreversibility in macroscopic response functions like these is a signature of metastability in the free energy landscape, that is, the existence of many local minima each of which represents a locally stable configuration of magnetic domains. The magnetization process essentially consists of a sequence of Barkhausen transitions between metastable states, each of which is inherently dissipative, activated by changes in field and temperature. Macroscopic response functions can provide a sensitive probe of the Barkhausen excitation spectrum, and the Preisach model of hysteresis offers the natural theoretical platform for such an interpretation. The model [30–33] resolves each metastable configuration into an ensemble of hypothetical two state subsystems, and each configuration is specified by listing all of the individual subsystem state assignments, although no spatial correlations between the subsystems and the domain pattern are implied. Each subsystem represents a cluster of spins of moment μ which is reversed cooperatively during a Barkhausen event, when the entire system evolves spontaneously from one metastable state to another, and each is characterized by a double well free energy landscape with two states $\varphi = \pm\mu$, a dissipation barrier $W_d = \mu H_d$, which measures the energy irreversibly dissipated as heat in a Barkhausen event, and a level splitting $W_s = 2\mu H_s$, which measures the energy stored reversibly in an event. Equivalently, the subsystems may be characterized by two free energy barriers to moment reversal $W_\pm = \mu(H_d \pm H_s)$, with critical excitation fields $\alpha = H_d - H_s$ and $\beta = -H_d - H_s$. Each subsystem has a history dependent response function with an upper branch $m_+ = (1-f)\mu \pm f\mu(1-\exp(-\lambda|H_a|))$ for $H_a \geq \beta$ and a lower branch $m_- = -(1-f)\mu \pm f\mu(1-\exp(-\lambda|H_a|))$ for $H_a \leq \alpha$, with $0 \leq f \leq 1$, where the second term represents the elastic component of the wall motion. A given magnetic material is characterized by a spectrum of dissipated and stored energies W_d and W_s which is represented by a distribution of characteristic fields, in this case, the product of a Lorentzian and a Gaussian:

$$p(H_d, H_s) = (\sigma_d/\pi)\left[(H_d - \bar{H}_d)^2 + \sigma_d^2\right]^{-1} \cdot (2\pi\sigma_s^2)^{-1/2} \exp(-H_s^2/2\sigma_s^2). \quad (4)$$

Thermal fluctuations reduce all free energy barriers by $W^*(T) = k_B T \ell n(t_{\exp}/\tau_0)$, where $t_{\exp}$ is the experimental measurement time constant and τ_0^{-1} is a fundamental characteristic frequency which is related to the curvature of the potential well [30]. Explicit variations in the characteristic energies W_d and W_s with temperature are modelled by allowing the spontaneous moment μ(T) and the parameters $\bar{H}_d(T)$, $\sigma_d(T)$, and $\sigma_s(T)$, which define the distribution of characteristic fields $p(H_d, H_s)$ to vary with temperature. The total moment M of the assembly in an external field H_a at temperature T is a history dependent, weighted sum of the responses from all of the individual Barkhausen subsystems:

$$M = \int_0^\infty dH_d \int_{-\infty}^{+\infty} dH_s \, m(H_d, H_s, H_a, T)\, p(H_d, H_s) \quad (5)$$

where the moment $m(H_d, H_s, H_a, T)$ of each subsystem assumes the values $m = m_+$, or $m = m_-$ or, if the element is in thermal equilibrium, $m = \mu\tanh[\mu(H_a + H_s)/k_B T]$. For a given field H_a and temperature T, the choice depends on the history of field and temperature excursions which characterize a specific experimental protocol. These are described in detail in reference [32], and will not be reproduced here.

Numerical simulations show [32] that the individual macroscopic response functions differ in their sensitivity to the two characteristic energies which define the double well free energy landscape. Thus, the field and temperature dependences of the ZFC moment and the hysteresis isotherms are determined primarily by the properties of the distribution of dissipation barriers, while the FC moment is most sensitive to the distribution of stored energies. These relationships have been exploited to generate numerical simulations of the response functions (solid curves in Figs. 4 and 5), and thus to quantify the spectrum of Barkhausen excitations. The numerical values of the fitting parameters are summarized in Table 1 and in Figure 6, which shows the temperature dependence of the Barkhausen moment $\mu(T)/\mu_0$, the most probable dissipation field $\bar{H}_d(T)/\bar{H}_{d0}$, the dispersion of dissipation fields $\sigma_d(T)/\sigma_{d0}$, and the dispersion of bias fields $\sigma_s(T)/\sigma_{s0}$, along with the thermal fluctuation field $W^*(T)/\bar{W}_d(0)$, and the measured coercive field $H_c/\bar{H}_{d0}$, all normalized to their zero temperature values. With the exception of a weak systematic upward trend in σ_{s0} with increasing field H_a and in λ with increasing temperature T (both of which are probably symptomatic of the oversimplified treatment of reversibility), it is possible to replicate all the principal features of the response in Figures 4 and 5 with a *single set* of parameter values.

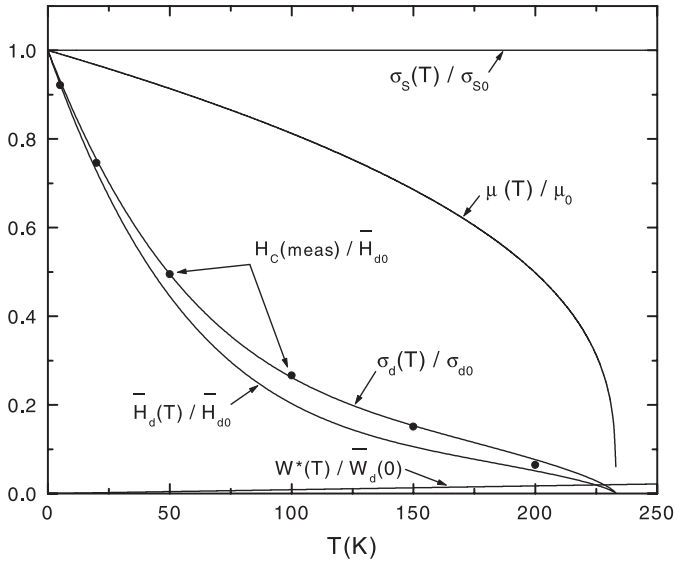

Fig. 6. The temperature dependence of the measured coercive field $H_c(\text{meas})/\bar{H}_{d0}$, and of the model parameters $\mu(T)/\mu_0$, $\bar{H}_d(T)/\bar{H}_{d0}$, $\sigma_d(T)/\sigma_{d0}$, $\sigma_s(T)/\sigma_{s0}$, and $W^*(T)/\bar{W}_d(0)$.

Table 1. Characteristic Parameters of the Barkhausen Spectrum of $La_{0.5}Sr_{0.5}CoO_3$.

μ_0 (emu)	$\geq 2.0 \times 10^{-14}$
$\bar{H}_{d0}$ (Oe)	$2000 \pm 5\%$
σ_{d0} (Oe)	$1100 \pm 5\%$
σ_{s0} (Oe)	$100 - 180 \pm 10\%$
f	$0.4 \pm 10\%$
λ (Oe^{-1})	$0.26 - 0.40 \pm 5\%$
M_{sat} (emu)	$3.3 \pm 10\%$
T_C (K)	$233 \pm 2\%$
$\ln(t_{\text{exp}}/\tau_0)$	25

The physical picture which emerges from the analysis may be summarized as follows: (1) In low applied fields $H_a < 100$ Oe, where the contribution from the elastic component is negligible, the thermal profile of the FC moment is essentially an undistorted image of the evolution of the Barkhausen moment $\mu(T)$ with temperature. This evolution may originate either from critical changes in the spontaneous moment or from the noncritical "growth" of the Barkhausen elements. In either case, the Barkhausen moment $\mu(T)$ vanishes as $T \rightarrow T_C$ and the magnetically ordered state dissolves, as expected. (2) In the same weak field limit, the field dependence of the FC moment at a fixed temperature T is defined almost exclusively by the characteristics of the distribution of bias fields $g(H_s)$. Assuming a Gaussian form for $g(H_s)$, the fits yield a dispersion $\sigma_{s0} \cong 150$ Oe, with a negligible temperature dependence. (3) Thermal fluctuations, which are represented in the model by the thermal viscosity field $H_T^* \equiv (k_B T/\mu(T)) \cdot \ell n(t_{\text{exp}}/\tau_0)$, play an insignificant role in defining the temperature dependence of the magnetic response in this system, except perhaps just below the critical temperature T_C, where the thermal field H_T^* begins to diverge. The ineffectiveness of thermal fluctuations is a reflection of the size of the Barkhausen elements, and the simulations were able to place a *lower bound* on the zero temperature Barkhausen moment μ_0 of $\mu_0 \geq 2.0 \times 10^{-14}$ emu. The $La_{0.5}Sr_{0.5}CoO_3$ system is a sintered granular material with, according to SEM measurements, a typical grain size of ~ 1 μm. Assuming an average Co moment of 2.5 μ_B, this yields a saturation moment per grain between $(2\text{–}5)\times 10^{-10}$ emu. Thus the lower limit on the Barkhausen moment is orders of magnitude less than the saturation moment of a grain (a result which is not sensitive to the specific value assumed for the average Co moment), which suggests that the Barkhausen excitations in this system probably originate from the motion of spatially localized domain wall fragments which are activated over local pinning barriers. (4) The ZFC response to a positive applied field H_a at any temperature T is due to the reversal of those Barkhausen elements which are trapped in their $\varphi = -\mu$ state during zero field cooling, and then excited into their $\varphi = +\mu$ state by a combination of field energy and thermal fluctuation energy. The activation condition for a Barkhausen element with characteristic fields (H_d, H_s) is $H_d(T) - H_s(T) < H_a + H_T^*$, so that the temperature dependence of the ZFC moment is defined by a combination of barrier growth, specifically $W_-(T) = \mu(T)(H_d(T) - H_s(T))$, and thermal relaxation $W^*(T) = k_B T \cdot \ell n(t_{\text{exp}}/\tau_0)$. In $La_{0.5}Sr_{0.5}CoO_3$, the contribution from thermal relaxation is negligible, and the growth of the ZFC moment which is observed in all fields in Figure 4 as the system is warmed from low temperatures through the ordered phase, originates entirely from the collapse of the Barkhausen dissipation barriers, although this trend is opposed, and eventually reversed at higher temperatures, by the collapse of the Barkhausen moment $\mu(T)$ itself as $T \rightarrow T_C$, leading to a maximum in $M_{ZFC}(T)$. (5) Similarly, none of the systematic changes observed in the major hysteresis loop in Figure 5 as the system is warmed through the ordered phase can be attributed to superparamagnetism, that is, to an increase in the population of Barkhausen elements which have reached thermal equilibrium and hence behave reversibly with respect to the application and removal of a field. Thus, the collapse of the coercive field is a direct consequence of the intrinsic collapse of the dissipation fields, as described by $\bar{H}_d(T)$ and $\sigma_d(T)$, while the drop in the saturation remanence simply reflects the collapse of the Barkhausen moment as $T \rightarrow T_C$.

4 Summary and conclusions

The analysis presented above shows that the $La_{0.5}Sr_{0.5}CoO_3$ system undergoes a continuous second order transition into a ferromagnetic state at a critical temperature $T_C = 230.9 \pm 0.2$ K. While the *effective* critical exponents, obtained from an analysis of the critical susceptibility maxima performed entirely above T_C, are *consistent* with both mean-field and Ising (plus dipole-dipole interaction) model predictions,

the fields required to ensure that the critical contribution to the susceptibility dominates that arising from regular (technical) sources are substantial ($\geq$1 kOe) (this dominance underlies this analysis, based on the application of equations (1–3)). Such conditions mean that these *effective* exponents *may not* be the same as the asymptotic ones; nevertheless the appearance of field and temperature dependent critical maxima (Fig. 1) are an unequivocal signature of a (continuous) transition to a ferromagnetic state. Below T_C, the system is composed of domains and the magnetic response is dominated by the field activated motion of domain wall fragments over local free energy pinning barriers. The maximum observed in the low field ZFC moment in Figure 4 and the sharp cusp observed in the zero field differential susceptibility in the insert in Figure 1 (the so-called Hopkinson effect) are both caused by a competition between the collapse of these free energy pinning barriers as the system is warmed through the ordered phase, which enhances the response, and the collapse of the Barkhausen moment as $T \rightarrow T_C$, which suppresses the response. Roughly speaking, the inflection point in the ZFC moment below the maximum corresponds to the temperature at which the applied field H_a activates the most probable pinning barrier $\bar{W}_d$. Thus the tendency for the maximum in the ZFC moment to shift to lower temperatures with increasing field H_a reflects the precise manner in which the free energy barriers grow with decreasing temperature, while the tendency for the maximum to become broader is a consequence of the expanding temperature range $(T_C - T_{infl})$ over which the ZFC response is dominated by the temperature dependence of the Barkhausen moment $\mu(T)$, which is quite slow except when T is very close to T_C. An analogous behaviour is observed in the temperature dependence of the differential susceptibility χ with changes in the static biasing field in Figure 1, and its physical origin is the same. The analysis also quantifies the distribution of energies *stored* reversibly in Barkhausen transitions, as represented by the double well level bias. These effects are subtle, particularly in ferromagnetic systems which tend to be dissipation dominated, and are encoded primarily in the amplitude and temperature dependence of the FC moment, where they compete (at higher fields) with elastic contributions to the response. In $La_{0.5}Sr_{0.5}CoO_3$, the bias fields are randomly distributed about zero with a dispersion σ_s which is essentially temperature independent, and only weakly dependent on applied field, varying from $\sigma_{so} \cong 100$ Oe at low fields $H_a \leq 100$ Oe to $\sigma_{so} \cong 180$ Oe in higher fields $H_a \geq 1000$ Oe.

In summary, the above analysis shows that $La_{0.5}Sr_{0.5}CoO_3$ can be described comprehensively as a ferromagnet with strong irreversibility. Preisach simulations show that the principal structural features of the irreversible response, namely the pronounced bifurcation of the FC and ZFC branches and the maximum in the ZFC moment just below T_C, are symptomatic of a distribution of energy barriers which collapse rapidly as $T \rightarrow T_C$, and for which moment reversal is field activated rather than thermally activated. From this perspective, the irreversible behaviour of $La_{0.5}Sr_{0.5}CoO_3$ is no different from that of conventional long-range ordered ferromagnets with domain structure like $SrRuO_3$ [34]. Thus FC/ZFC bifurcation coupled with a ZFC maximum are generic features of all systems with a corrugated free energy landscape, and are *not* signatures of glassy magnetic structure, contrary to recent speculations [5] which attempt to invoke these structural elements as partial evidence for magnetic phase separation, or to relate them to de Almeida-Thouless instabilities [9,36]. (As mentioned earlier, anomalies in the dynamic response have been interpreted [5,9] as evidence of cluster glass freezing at a temperature $T_f < T_C$. However, these authors also concede [5] that these finite clusters *percolate* into an "infinite" ferromagnetic "backbone" for Sr concentrations $x \geq 0.2$. For canonical percolating systems like AuFe [37], the formation of the infinite "backbone" is independent of the cooling protocol (FC versus ZFC), and the dynamic anomalies are associated with finite clusters which have not merged with the infinite "backbone". While the notion of percolation which is induced by field cooling, but not by zero field cooling [5], may be appealing as an explanation of colossal magnetoresistance effects (notwithstanding the extremely subtle energy balance which must be involved), it is not consistent with the present analysis, or indeed that of canonical "reentrant" systems like AuFe [37].) Furthermore, the simulations are able to replicate the measured irreversible response without invoking any reentrant mechanisms, and are thus consistent with the most recent predictions regarding the absence of an equilibrium ferromagnetic-spin glass phase transition in three dimensions [35].

The authors would like to acknowledge the financial support of the Natural Sciences and Engineering Research Council of Canada.

References

1. A.P. Ramirez, J. Phys.: Condens. Matter **9**, 8171 (1997); *Colossal Magnetoresistive Oxides* (edited by Y. Tokura) (Gordon and Breach, Amsterdam, 2000)
2. R. Caciuffo, D. Rinaldi, G. Barucca, J. Mira, J. Rivas, M. A. Senaris-Rodriguez, P. G. Radaelli, D. Fiorani, J.B. Goodenough, Phys. Rev. B **59**, 1068 (1999); Europhys. Lett. **45**, 399 (1999); R. Mahendiran, A.K. Raychaudhuri, Phys. Rev. B **54**, 16044 (1996); B.I. Belevtsev, N.T. Cherpak, I.N. Chukanova, A.I. Gubin, V.B. Krasovitsky, A.A. Lavrinovich, J. Phys.: Condens. Matter **14**, 2591 (2002)
3. P. Ganguly, P.S.A. Kumar, P.N. Santhosh, I.S. Mulla, J. Phys.: Condens. Matter **6**, 533 (1994); S. Mukherjee, R. Ranganathan, P.S. Anil Kumar, P.A. Joy, Phys. Rev. B **54**, 9267 (1996)
4. G. Baio, G. Barucca, R. Caciuffo, D. Rinaldi, J. Mira, J. Rivas, M.A. Senaris-Rodriguez, D. Fiorani, J. Phys.: Condens. Matter **12**, 9761 (2000)
5. J. Wu, C. Leighton, Phys. Rev. B **67**, 174408 (2003)
6. D. Kim, B.L. Zink, F. Hellman, J.M.D. Coey, Phys. Rev. B **65**, 214424 (2002)

7. V.G. Sathe, A.V. Pimpale, V. Siruguri, S.K. Paranjpe, J. Phys.: Condens. Matter **8**, 3889 (1996)
8. S. Tsubouchi, T. Kyôman, M. Itoh, Phys. Rev. B **67**, 094437 (2003)
9. D.N.H. Nam, K. Jonason, P. Nordblad, N.V. Khiem, N.X. Phuc, Phys. Rev. B **59**, 4189 (1999)
10. P.A. Joy, P.S. Anil Kumar, S.K. Date, J. Phys.: Condens. Matter **10**, 11049 (1998)
11. N. Menyuk, P.M. Raccah, K. Dwight, Phys. Rev. **166**, 510 (1968)
12. S. Madhukar, S. Aggarwal, A.M. Dhote, R. Ramesh, A. Krishnan, D. Keeble, A. Poindexter, J. Appl. Phys. **81**, 3543 (1997)
13. S. Chikazumi, *Physics of Ferromagnetism* (Clarendon, Oxford, 1997); T. Nagata, *Rock Magnetism* (Plenum, NY, 1961)
14. H.P. Kunkel, R.M. Roshko, G. Williams, Phys. Rev. B **37**, 5880 (1988)
15. H.E. Stanley, *Introduction to Phase Transitions and Critical Phenomena* (Clarendon, Oxford, 1971); G. Williams, in *Magnetic Susceptibility of Superconductors and Other Spin Systems*, edited by R.A. Hein et al. (Plenum, New York, 1991)
16. M. Campostrini, M. Hasenbusch, A. Pelissetto, P. Rossi, E. Vicari, Phys. Rev. B **65**, 144520 (2002)
17. R.M. Roshko, G. Williams, J. Phys. F **14**, 703 (1984)
18. G. Williams, *Proceedings of the International Conference on Magnetic Materials* (Calcutta, 2000), J. Alloys Comp. **326**, 36 (2001)
19. J.H. Zhao, T. Song, H.P. Kunkel, X.Z. Zhou, R.M. Roshko, G. Williams, J. Phys.: Condens. Matter **12**, 6903 (2000); J.H. Zhao, H.P. Kunkel, X.Z. Zhou, G. Williams, J. Phys.: Condens. Matter **13**, 9349 (2001); J.H. Zhao, H.P. Kunkel, X.Z. Zhou, G. Williams, Phys. Rev. B **59**, 8391 (1999); X.Z. Zhou, H.P. Kunkel, J.H. Zhao, P.A. Stampe, G. Williams, Phys. Rev. B **56**, R12714 (1997)
20. J.H. Zhao, H.P. Kunkel, X.Z. Zhou, G. Williams, M.A. Subramaniam, Phys. Rev. Lett. **83**, 219 (1999)
21. J. Mira, J. Rivas, M. Vazquez, J.M. Garcia-Beneytez, J. Arcas, R.D. Sanchez, M.A. Senaris-Rodriguez, Phys. Rev. B **59**, 123 (1999)
22. J.A. Osborn, Phys. Rev. **67**, 35 (1945). Past experience has shown that this numerical estimate places an upper limit on N; indeed the zero-field susceptibility maximum evident in the insert in Figure 1 represents less than 1% of the demagnetisation limit, so estimated. This result is consistent with the absence of shearing curve behaviour in the field dependence of the magnetisation, mentioned above. Furthermore we do *not* adjust the value for N such that the demagnetisation factor corrected susceptibility – the true susceptibility – diverges at T_C, as this would lead to spurious behaviour. This failure to reach the demagnetisation limit is a common feature of ferromagnets with strong irreversibility – see, for example, P.A. Stampe, G. Williams, J. Phys.: Condens. Matter **10**, 6771 (1998)
23. This procedure yields a straight line, so the extrapolation to $H_i = 0$ is straightforward. Small adjustments, ΔT_C, in $T_C(\Delta T_C/T_C \sim 2 - 4 \times 10^{-3})$ are admitted until a consistent set of plots associated with equations (2) and (3) are obtained. For the present system, it turns out that Heisenberg model exponents $(\gamma + \beta)^{-1} = 0.57$ produce a satisfactory alternative to Figure 3a using $T_C = 229.7 \pm 0.2$ K (found using the same extrapolation technique discussed above, but with the appropriate $(\gamma + \beta)^{-1}$ value). However, this latter choice for T_C yield $\gamma = 1.09 \pm 0.02$ for the equivalent of Figure 3b; this estimate is closer to the mean-field value and clearly inconsistent with Heisenberg model predictions
24. Z. Wang, H.P. Kunkel, G. Williams, J. Phys.: Condens. Matter **4**, 10385 (1992)
25. A. Aharony, Phys. Rev. B **8**, 3363 (1973)
26. J.L. Alonso, L.A. Fernández, F. Guinea, V. Laniena, V. Martin-Mayor, Nucl. Phys. B **596**, 587 (2001)
27. M. Ziese, J. Phys.: Condens. Matter **13**, 2919 (2001)
28. Ch.V. Mohan, M. Seeger, H. Kronmüller, P. Murugaraj, J. Maier, J. Magn. Magn. Mater. **183**, 348 (1998)
29. K. Ghosh, C.J. Lobb, R.L. Greene, S.G. Karabashev, D.A. Shulyatev, A.A. Arsenov, Y. Mukovskii, Phys. Rev. Lett. **81**, 4740 (1998)
30. J.J. Prejean, J. Souletie, J. Phys. France **41**, 1335 (1980)
31. J. Souletie, J. Phys. France **44**, 1095 (1983)
32. T. Song, R.M. Roshko, E.D. Dahlberg, J. Phys.: Condens. Matter **13**, 3443 (2001)
33. G. Bertotti, *Hysteresis in Magnetism* (Academic Press, 1998)
34. R.M. Roshko, D.L. Huo, Physica B **306**, 246 (2001)
35. F. Krzakala, O.C. Martin, Phys. Rev. Lett. **89**, 267202-4 (2002)
36. J. de Almeida, D. Thouless, J. Phys. A **11**, 983 (1978)
37. B.R. Coles, B.V.B. Sarkissian, R.H. Taylor, Phil. Mag. **37**, 489 (1978)